Exploring Feature Coupling and Model Coupling for Image Source Identification

Yonggang Huang, *Member, IEEE,* Longbing Cao, *Senior Member, IEEE,*
Jun Zhang, *Member, IEEE,* and Yuying Liu

***Abstract*—Recently, there has been a great interest in feature based image source identification. Previous statistical learning based methods usually defined the identification process as a classification problem. They assumed the dependence of features and the dependence of models. However, the two assumption are usually problematic, because of the genuine coupling of features and models. To address the two issues, in this paper, we propose a new image source identification scheme. For the feature coupling, a coupled feature representation is adopted to analyze the coupled interaction among features. The coupling relations among features and their powers are quantified with Pearson's correlations, and integrated in a Taylor-like expansion manner. Regarding model coupling, a new coupled model probability representation is developed. The model coupling relationships are characterized with conditional probabilities induced by confusion matrix. The conditional probabilities are then combined with the law of total probability. The experiments carried out on the Dresden image collection confirm the effectiveness of the proposed scheme. Via mining the feature coupling and model coupling, the identification accuracy can be significantly improved.**

***Index Terms*—Image source identification, feature coupling, model coupling, machine learning, digital forensics.**

I. Introduction

WITH the pervasive connectivity and availability of the Internet and digital imaging technologies, massive digital images are created and used in everyday's life. Nowadays, more and more governmental, legal, scientific organizations use digital images as crucial evidence to make decisions [1]. Source identification is one of the most fundamental requirements in these scenarios, which aims to associate an image with its acquisition device. For example, identifying source device of child abuse images in court, verifying the owner of images for copyright disputing [2].

Existing source identification approaches can be classified into three categories. The apparent simple solution is the *image metadata based* approach, which is to investigate the EXIF (Exchangeable Image File) header [3] of an image. The image source related information, such as camera brand, model, are directly embedded in the EXIF header. However, the metadata based solution is unreliable in practice, since the EXIF header can be easily manipulated. The *watermark based* approach [4, 5] addresses the issue of source identification via inserting into the image a watermark. The watermark carries the source related information. However, the watermark injection module can increase the production cost of digital cameras. Recently, researchers have been devoted to the *feature based* approach [6–10]. Firstly, features on hardware or software-related fingerprints left during the image acquisition process are extracted. Then, the source identification is regarded as classification problem and solved with statistical classifiers such as support vector machine (SVM) [11]. In this paper, we focus on the feature based approach.

Traditional feature based approach usually assume the independence of features and the independence of models. That is, the extracted features are directly feed into the statistical classifiers without mining their relationships. Moreover, the output labels of classifier are straightforward used as identification results, without further considering the relationships among source models. However, the feature independence and model independence assumptions are usually problematic, because of the genuine coupling of both features and models.

- *Feature Coupling*: The features characterize the hardware or software-related fingerprints from different views, they are naturally related to each other in certain ways. For example, the Average Pixel Value and Neighbor Distribution Center of Mass features both describe pixel distributions of different color bands with different views, those features tend to have the related distributions.
- *Model Coupling*: The camera models designed by the same manufacturer tend to be related to each other, because those models may have the analogous hardware infrastructure and similar image processing algorithms. As an example, the models *Agfa_DC-504* and *Agfa_Sensor530s* tend to couple with each other, and the identification results of the two models could be mixed up.

This work is to investigate the issues of feature coupling and model coupling for image source identification. Our goal is to design a new image source identification scheme which can capture both the feature coupling and model coupling relationships. The major contributions of our work are summarized as follows.

- To the best of our knowledge, our work is the first to identify and address the issues of feature coupling and model coupling for source camera identification.
- We design a new image source identification scheme, which can capture the feature coupling via coupled fea-

Y. Huang and Y. Liu are with School of Computer Science and Technology, Beijing Institute of Technology, Beijing, 100081, China (e-mail: yonggang.h@gmail.com, liuyuying0205@163.com)

L. Cao is with Faculty of Engineering and Information Technology, University of Technology Sydney, New South Wales, 2007, Australia (e-mail: longbing.cao@uts.edu.au)

J. Zhang is with School of Information Technology, Deakin University, VIC, 3217, Australia (e-mail: jun.zhang@deakin.edu.au)

Manuscript received XX XX, 2017; revised XX XX, 2017.

ture representation, and the model coupling by coupled model probability representation.
- A novel coupled feature representation is employed to analyze the coupled interaction among features, which can successfully capture the intrinsic linear and non-linear coupling relationships. The coupling relations among features and their powers are quantified with Pearson's correlations, and integrated in a Taylor-like expansion manner.
- We propose a new coupled model probability representation to capture the dependence relationships among source models. The model coupling relationships are characterized with conditional probabilities induced by confusion matrix. The conditional probabilities are then combined following the law of total probability.

The remainder of the paper is structured as follows. Some related work is briefly reviewed in Section II. Section III demonstrates the feature coupling and model coupling phenomenons on a real-world dataset. Section IV presents the new image source identification scheme in detail. Section V reports the experiments and results. Finally, the paper is concluded in Section VI.

II. Related work

Recently, researchers have been devoted on the feature based image source identification solutions [6–10]. Existing research efforts can be classified into two categories. The first is to design sophisticated features to capture the fingerprints left during the image acquisition process. Based on these features, the second category of researches focus on developing novel statistical leaning based identification solutions.

To our best knowledge, both the problems of feature coupling and model coupling haven't been addressed in existing researches on feature based image source identification.

A. Features of Image Source Identification

Research efforts of this category aim to design various features to capture the intrinsic hardware artifacts and software-related fingerprints left during the image acquisition process. The pattern noise [12–18], lens radial distortion [19–21], chromatic aberration [22], and sensor dust [23, 24] are the typical features of hardware artifacts. Image-related features [7] and artifacts introduced by color filter array [6] are two representatives of software-related features.

Kharrazi *et al.*s work [7] is the first endeavor in this domain. Their work was motivated by the observation that an output image is greatly effected by the color filter arrays demosaicing algorithm and color transformation. In their research, 34 features were developed to capture the underlying color characteristics of different cameras. The hot pixels or dead pixels are treated as evidence for source camera identification in Geradts *et al.*'s work [25]. Dirik *et al.* [23] observed that dust spots can be a useful fingerprint for digital single lens reflex cameras, and they developed a novel image source identification method based on sensor dust traces. Choi *et al.*'s solution [19] was motivated by the observation that the majority of digital cameras are equipped with lenses having spherical surfaces, whose inherent radial distortions serve as unique fingerprints. They used intrinsic lens radial distortion for image source identification. In literature [22], Van *et al.* estimated the parameters of lateral chromatic aberration and used them as features for camera identification. The underline idea is the chromatic aberration phenomenon, where lights of different wavelengths fail to converge at the same position on the focal plane. Several researches have been focused on using the photo-response nonuniformity noise (PRNU) as fingerprint for camera identification. Lukáš *et al.*'s effort [12] is the first step towards this direction. In their approach, firstly, original images are denoised with a wavelet denoising filter to attain PRNU. Then, by averaging the PRNU of images, the reference PRNU of the camera can be obtained. Finally, the correction between PRNU of an image and the camera reference PRNU was used to perform the image source identification. Li *et al.* [15] argued that color filter array can lead to inaccurate extraction of PRNU. To address this issue, they decomposed each color channel into four sub-images and extracted the PRNU from each sub-image. The PRNU of the sub-images are then combined.

Most recently, Convolutional Neural Networks (CNNs) is used to extract feature for image source identification [26–28]. Different from previous works replying on hand-crafted descriptors, the CNNs based manner [26–28] takes advantage of great amount of data in order to learn characteristic features directly from the data itself. In other words, that is purely data-driven.

B. Statistical Leaning based Image Source Identification

After feature extraction, image source identification can be treated as machine learning problem and solved with statistical learning tools. Existing research works towards this direction can be classified into two categories: *supervised learning* based approaches and *unsupervised learning* based approaches.

In the supervised learning based approaches, images from a number of known camera models are collected in advance, and the target images are assumed to be from one of the given camera models. In this situation, image source identification is treated as a K-class (K is the number of known models) classification problem, and solved with multi-class classifiers such as multi-class SVM [6–10]. In a more challenging open set scenario, the target images may also come from unknown sources. The key is how to identify images of the unknown models as well as distinguish the images of the known models [29, 30]. Costa *et al.* [29] proposed a decision boundary carving based approach (DBC) to deal with unknown models. Regarding the images of a known model as positive samples and the images of other known models as negative samples, a binary SVM is trained. Taking unknown models into account, the decision boundary of the SVM is adjusted towards the positive class and outwards the negative class to minimize future false positive matches. Huang *et al.* [30] propose a new scheme, namely Source Camera Identification with Unknown models (SCIU), to address the problem of unknown. SCIU can explore the information of unknown models through unknown detection and unknown expansion, and then incorporate the unknown information into the $(K + 1)$-class classification.

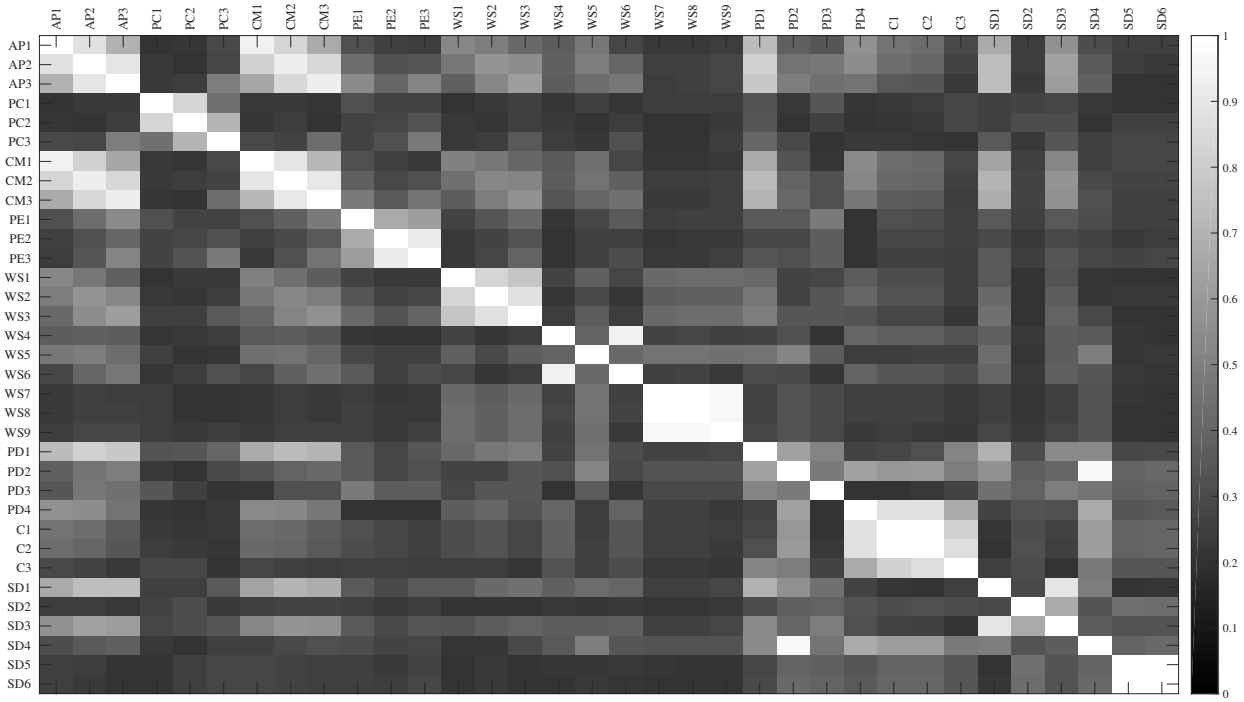

Fig. 1: The coupling relationships of the 34 features (For clarity, the absolute value of Pearson's correction coefficient is showed.)

In the unsupervised learning based approaches, the prior information on the possible sources involved is unavailable. In this scenario, the issue is to understand which images are from the same camera models, and which are not. In previous researches, clustering technologies are usually employed to address this problem. Bloy [31] is the pioneer of this direction. He proposed using pairwise nearest neighbor (PNN) algorithm to deal with this problem. Boly introduced some tricks into PNN for reducing computation cost, such as randomly picking clusters candidates for merging. To further alleviate the computational burden, some variants of this procedure can be found in literatures [32, 33]. Some researchers [34, 35] regarded this issue as a graph partitioning problem. The images were treated as nodes in a weighted undirected graph, graph processing tools were then used to partition the graph into disjunct sets. Most recently, Marra *et al.* [36] developed a new purely blind clustering method leveraging correction clustering, consensus clustering and ad hoc cluster refinement. A remarkable feature of the new method is that it does not require the user to set critical parameters, such as the number of clusters, or some thresholds on data similarity.

III. Coupling Phenomenons

In this section, we show the genuine coupling phenomenons with experimental results on a real-world dataset.

A. Feature Coupling

The features are designed to capture the fingerprints left during the image acquisition process. Various features characterize the fingerprints from different views, therefore they are naturally coupled to each other. This couple relationship can be measured with the Pearson's correction coefficient [37].

Given the features f_i and f_j, the image collection Φ, the Pearson's correction coefficient of f_i and f_j can be calculated as,

$$Cor(f_i, f_j) = \frac{\sum_{I\in\Phi}(f_i(I) - \bar{f}_i)(f_j(I) - \bar{f}_j)}{\sqrt{\sum_{I\in\Phi}(f_i(I) - \bar{f}_i)^2}\sqrt{\sum_{I\in\Phi}(f_j(I) - \bar{f}_j)^2}}, \quad (1)$$

where I is an image in Φ, $f_i(I)$ denotes the feature value of I on f_i. $\bar{f}_i$, $\bar{f}_j$ represent the mean value of f_i and f_j on Φ respectively.

Suppose the feature set is $\mathbb{F} = \{f_1, \cdots, f_F\}$. The pairwise coupling relationships of features in $\mathbb{F}$ can be represented as feature coupling matrix as

$$FCM = \begin{pmatrix} Cor(f_1, f_1) & Cor(f_1, f_2) & \cdots & Cor(f_1, f_F) \\ Cor(f_2, f_1) & Cor(f_2, f_2) & \cdots & Cor(f_2, f_F) \\ \vdots & \vdots & \ddots & \vdots \\ Cor(f_F, f_1) & Cor(f_F, f_2) & \cdots & Cor(f_F, f_F) \end{pmatrix}. \quad (2)$$

Figure.1 shows the feature coupling matrix of 34 features with grey-scale map. The experiment setting here is the same with that in Section.V-A, and the experiment was performed on set C. We can see that some features are closely coupled

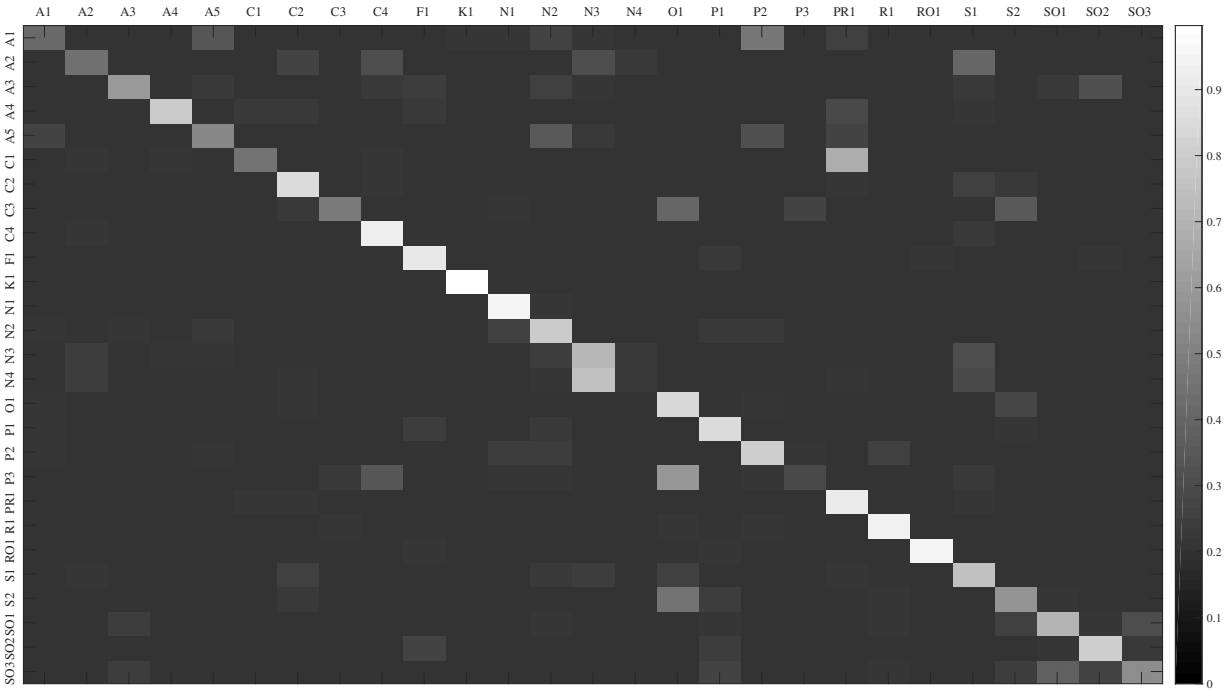

Fig. 2: The coupling relationships of the 27 models.

to each other. Some representatives of coupled feature pairs are as follows.

- AP2 (Average Pixel Value, channel G) and AP3 (Average Pixel Value, channel B). The two features are both based on the gray world assumption, and they are calculated in the same manner.
- AP1 (Average Pixel Value,channel R) and CM1 (Neighbor Distribution Center of Mass, channel R). AP1 and CM1 are both captured in the red channel.
- AP3 (Average Pixel Value, channel B) and CM3 (Neighbor Distribution Center of Mass, channel B). The two features are obtained from the blue band.

B. Model Coupling

The camera models with the similar hardware infrastructures or image processing algorithms tend to be coupled with each other. In the identification task, the images from the two models tend to be mixed up. In this paper, we evaluate this coupling phenomenon based on confusion matrix.

Suppose the model set is $\mathbb{C} = \{C_1, \cdots, C_N\}$, the confusion matrix is defined as,

$$\begin{pmatrix} c_{11} & c_{12} & \cdots & c_{1N} \\ c_{21} & c_{22} & \cdots & c_{2N} \\ \vdots & \vdots & \ddots & \vdots \\ c_{N1} & c_{N2} & \cdots & c_{NN} \end{pmatrix}, \tag{3}$$

where c_{ij} is the count of images known to be from model C_i but predicted to be from model C_j. The counts can be normalised to percentages as,

$$\rho_{ij} = \frac{c_{ij}}{\sum_{k=1}^{N} c_{ik}}, \tag{4}$$

where ρ_{ij} is the percentage of images actually from model C_i but predicted to be from model C_j. Then, the coupling relationships of models can be denoted as model coupling matrix,

$$MCM = \begin{pmatrix} \rho_{11} & \rho_{12} & \cdots & \rho_{1N} \\ \rho_{21} & \rho_{22} & \cdots & \rho_{2N} \\ \vdots & \vdots & \ddots & \vdots \\ \rho_{N1} & \rho_{N2} & \cdots & \rho_{NN} \end{pmatrix}. \tag{5}$$

The grey-scale map of the model coupling matrix is presented in Figure.2. The experiment set-up is consistent with that in Section.V-A. The experiment was carried out on set C with the original feature representation, and the confusion matrix was obtained on the testing dataset. We can see that some camera models produced by the same manufacture are closely coupled to each other. For example, A1 (*Agfa_DC-504*) and A5 (*Agfa_Sensor530s*), SO1 (*Sony_DSC-H50*) and SO3 (*Sony_DSC-W170*). An interesting observation is that camera models of different manufactures may also be closely coupled. For instance, C1 (*Canon_Ixus55*) and PR1 (*Praktica_DCZ5.9*), S2 (*Samsung_NV15*) and O1 (*Olympus_mju_1050SW*).

IV. Proposed Scheme

This section provides a detailed presentation of the proposed scheme. The system model of the new scheme is presented

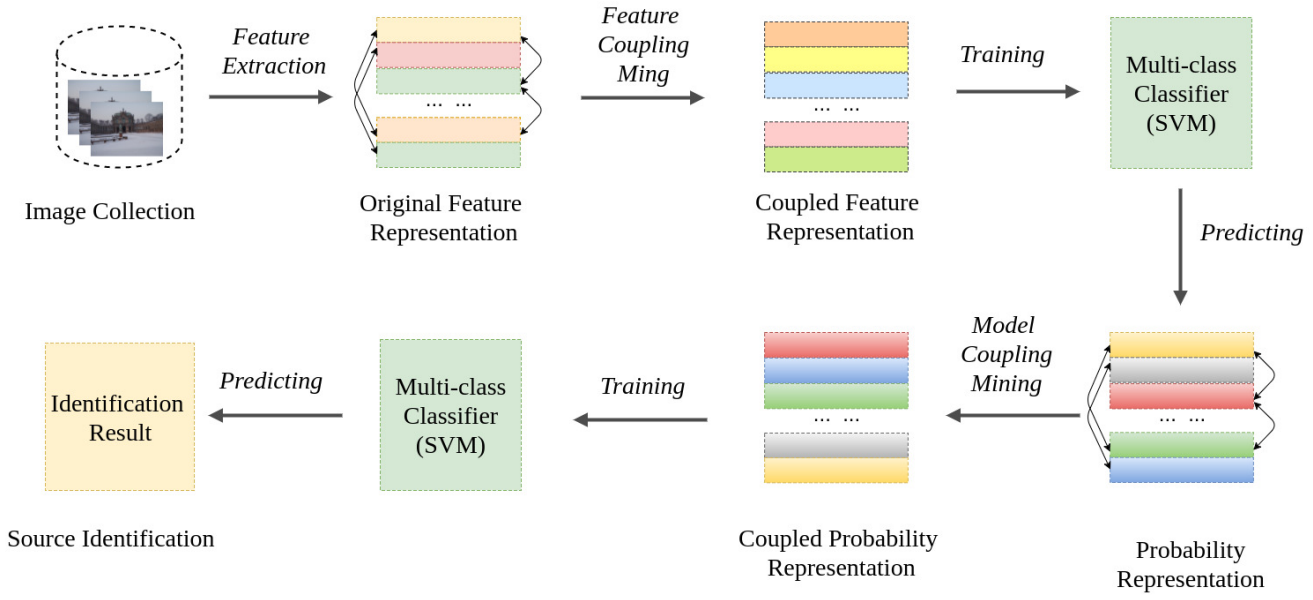

Fig. 3: The system model of the proposed scheme.

in Fig.3. As shown in the figure, the work flow of the new solution is as follows:

1) *Original Feature Representation*: The original features of the images in the image collection are extracted.
2) *Coupled Feature Representation*: The original features are mapped to coupled feature representation via mining feature coupling.
3) *Probability Representation*: The training samples with the coupled feature representation are firstly used to train multi-class classifier. Then, the trained classifier are used to classify all the samples, outputting the probabilities of being produced by each model. In this way, each sample is associated with a probability representation.
4) *Coupled Probability Representation*: By incorporating the model coupling relationships in the training dataset, the probability representation is converted to the coupled probability representation.
5) *Source Identification*: Finally, the identification classifier is trained using the training samples in the coupled probability representation, and then used to predict the testing samples.

Coupled feature representation and coupled probability representation are the two core components of the scheme, which will be depicted in detail in the following subsections.

A. Coupled Feature Representation

To the best of our knowledge, previous researches on image source identification [6–10] directly performed the classification task using the original image features, overlook the feature coupling relationships as shown in Section III-A. Motivated by the coupled object analysis strategies [38, 39] in the field of data mining, in our work, we propose to use coupled feature representation to capture this feature coupling relationships. The underline idea is to firstly expand features with their powers. Then, the coupling relations among features and their expansion are quantified with Pearson's correlations. Finally, the coupling relations are integrated with a Taylor-like expansion manner. In this way, both the linear and non-linear coupling relationships can be captured in the coupled feature representation. Particularly, both intra-feature coupling and inter-feature coupling relationships are taken into consideration.

Since the Pearson's correlation coefficient can describe the linear relationship between two features. In order to deeply investigate the coupling relationships, such as quadratic and cubic relationships, we expand features with their powers. Given feature f_i, the expansion can be expressed as a feature vector,

$$\vec{f_i} = [f_i^1, \cdots, f_i^t, \cdots, f_i^T], \tag{6}$$

where f_i^t is the t-th power of f_i, and T is the largest power.

Two types of coupling relationships are taken into consideration for coupled feature representation. One is the *intra-feature coupling*, which captures the coupling relationships of a feature and its expansion. The other is the *inter-feature coupling*, which focuses on calculating the coupling information of a feature and the expansion of other features.

We firstly consider the intra-feature coupling relationship. The relationship of f_i^t and f_i^s can be described with the Pearson's correction coefficient as,

$$\alpha(f_i^t, f_i^s) = Cor(f_i^t, f_i^s), \tag{7}$$

where $Cor(\cdot,\cdot)$ is defined in Formula.1.

Furthermore, the coupling relationships of f_i^t and $\vec{f_i}$ can be expressed as a coupling vector,

$$\alpha(f_i^t, \vec{f_i}) = [\alpha(f_i^t, f_i^1), \cdots, \alpha(f_i^t, f_i^T)]. \tag{8}$$

Then intra-feature coupling gain of $\vec{f_i}$ to f_i^t can be combined

in Taylor-like expansion manner as,

$$CG1(f_i^t|\vec{f}_i) = \frac{\alpha(f_i^t, f_i^1)}{1!} f_i^1 + \frac{\alpha(f_i^t, f_i^2)}{2!} f_i^2 + \cdots + \frac{\alpha(f_i^t, f_i^T)}{T!} f_i^T = \mathbf{w} \cdot \alpha(f_i^t, \vec{f}_i) \cdot \vec{f}_i, \tag{9}$$

where $\mathbf{w} = [\frac{1}{1!}, \frac{1}{2!}, \cdots, \frac{1}{T!}]$ is the constant weight vector. The underline idea of Taylor-like combination is that the features with larger powers should have less coupling gain contribution. That is, the s-th power of feature f_i^s is scaled with $\frac{1}{s!}$.

We further calculate the inter-feature coupling gain. The relationship of f_i^t and f_j^s $(j \neq i)$ can be described according to Formula.1 as,

$$\beta(f_i^t, f_j^s) = Cor(f_i^t, f_j^s). \tag{10}$$

The coupling relationships of f_i^t and $\vec{f}_j$ can be expressed as,

$$\beta(f_i^t, \vec{f}_j) = [\beta(f_i^t, f_j^1), \cdots, \beta(f_i^t, f_j^T)]. \tag{11}$$

Then, the inter-feature coupling gain of $\vec{f}_j$ contributing to f_i^t can be incorporated as,

$$CG2(f_i^t|\vec{f}_j) = \frac{\beta(f_i^t, f_j^1)}{1!} f_j^1 + \frac{\beta(f_i^t, f_j^2)}{2!} f_j^2 + \cdots + \frac{\beta(f_i^t, f_j^T)}{T!} f_j^T = \mathbf{w} \cdot \beta(f_i^t, \vec{f}_i) \cdot \vec{f}_j \tag{12}$$

Taking both the intra-feature coupling and inter-feature coupling into account, we have the synthetic coupled feature representation of f_i^t as,

$$\begin{aligned} CR(f_i^t) &= f_i^t + CG1(f_i^t|\vec{f}_i) + \sum_{j=1, j\neq i}^{F} CG2(f_i^t|\vec{f}_j) \\ &= f_i^t + \frac{\alpha(f_i^t, f_i^1)}{1!} f_i^1 + \frac{\alpha(f_i^t, f_i^2)}{2!} f_i^2 + \cdots + \frac{\alpha(f_i^t, f_i^T)}{T!} f_i^T \\ &+ \sum_{j=1, j\neq i}^{F} \frac{\beta(f_i^t, f_j^1)}{1!} f_j^1 + \sum_{j=1, j\neq i}^{F} \frac{\beta(f_i^t, f_j^2)}{2!} f_j^2 + \cdots + \sum_{j=1, j\neq i}^{F} \frac{\beta(f_i^t, f_j^T)}{T!} f_j^T \\ &= f_i^t + \mathbf{w} \cdot \alpha(f_i^t, \vec{f}_i) \cdot \vec{f}_i \\ &+ \overbrace{[\mathbf{w}, \cdots, \mathbf{w}]}^{F-1} \cdot [\beta(f_i^t, \vec{f}_1), \cdots, \beta(f_i^t, \vec{f_{i-1}}), \beta(f_i^t, \vec{f_{i+1}}), \cdots, \beta(f_i^t, \vec{f}_1)] \\ &\cdot [\vec{f}_1, \cdots, \vec{f_{i-1}}, \vec{f_{i+1}}, \cdots, \vec{f}_F]. \end{aligned} \tag{13}$$

Given the feature set $\mathbb{F} = \{f_1, \cdots, f_F\}$, we define,

$$\mathbb{F}_{-i} = \mathbb{F} - \{f_i\} = \{f_1, \cdots, f_{i-1}, f_{i+1}, \cdots, f_F\}. \tag{14}$$

Accordingly,

$$\vec{\mathbb{F}_{-i}} = [\vec{f}_1, \cdots, \vec{f_{i-1}}, \vec{f_{i+1}}, \cdots, \vec{f}_F], \tag{15}$$

and

$$\beta(f_i^t, \vec{\mathbb{F}_{-i}}) = [\beta(f_i^t, \vec{f}_1), \cdots, \beta(f_i^t, \vec{f_{i-1}}), \beta(f_i^t, \vec{f_{i+1}}), \cdots, \beta(f_i^t, \vec{f}_F)]. \tag{16}$$

Then, Formula.13 can be rewritten as,

$$\begin{aligned} CR(f_i^t) &= f_i^t + CG1(f_i^t|\vec{f}_i) + \sum_{j=1, j\neq i}^{F} CG2(f_i^t|\vec{f}_j) \\ &= f_i^t + \mathbf{w} \cdot \alpha(f_i^t, \vec{f}_i) \cdot \vec{f}_i + \overbrace{[\mathbf{w}, \cdots, \mathbf{w}]}^{F-1} \cdot \beta(f_i^t, \vec{\mathbb{F}_{-i}}) \cdot \vec{\mathbb{F}_{-i}}. \end{aligned} \tag{17}$$

Accordingly, the coupled feature representation of feature f_i's expansion is,

$$CR(\vec{f}_i) = [CR(f_i^1), \cdots, CR(f_i^T)] \tag{18}$$

Finally, when all the F original features are considered, we obtain the coupled feature representation to be a concatenated vector:

$$CR(\vec{\mathbb{F}}) = [CR(\vec{f}_1), \cdots, CR(\vec{f}_F)], \tag{19}$$

where $\vec{\mathbb{F}} = [\vec{f}_1, \cdots, \vec{f}_F]$.

B. Coupled Probability Representation

As shown in Section.III-B, because of the model coupling relationships, the identification results from the coupled models tend to be mixed up. Existing researches [6–10] directly use the outputs of identification classifier as final results, without considering the model coupling relationships. In this paper, a new coupled probability representation is proposed to capture the dependence relationships among source models. Firstly, via making use of the confusion matrix, the model coupling relationships are characterized with conditional probabilities. Then, conditional probabilities are combined following the law of total probability.

Previous researches [6–10] usually use the output labels of identification classifier (usually multi-class SVM) as identification results. Instead, we make use of the output probabilities of the classifier. The commonly used SVM implementation, LIBSVM [40], supports multi-class probability estimation via pairwise coupling [41].

Given the training dataset $\mathbb{T}$, the collection of all images Φ, and the model set $\mathbb{C} = \{C_1, \cdots, C_N\}$. Suppose the SVM model trained on $\mathbb{T}$ is $\mathbb{M}$, each sample I in Φ can be associated with a probability representation as,

$$\vec{e}(I) = [e_1(I), \cdots, e_N(I)] \leftarrow \mathsf{SVMPredict}(\mathbb{M}, I), \tag{20}$$

where $e_i(I)$ indicates the I's predicted probability of being from C_i.

As shown in Section.III-B, the model coupling relationships can be described with the confusion matrix. Taking this point into account, we use the conditional probability driven from the confusion matrix to characterize the model coupling. The SVM model $\mathbb{M}$ can be used to predict the images in training dataset $\mathbb{T}$, and the confusion matrix of the identification result can be represented as,

$$\begin{pmatrix} c_{11} & c_{12} & \cdots & c_{1N} \\ c_{21} & c_{22} & \cdots & c_{2N} \\ \vdots & \vdots & \ddots & \vdots \\ c_{N1} & c_{N2} & \cdots & c_{NN} \end{pmatrix}, \tag{21}$$

No.	Model	Size	Alias	No.	Model	Size	Alias	No.	Model	Size	Alias
1	Agfa_DC – 504	169	A1	10	FujiFilm_FinePixJ50	630	F1	19	Pentax_OptioW60	192	P3
2	Agfa_DC – 733s	281	A2	11	Kodak_M1063	2391	K1	20	Praktica_DCZ5.9	1019	PR1
3	Agfa_DC – 830i	363	A3	12	Nikon_CoolPixS710	925	N1	21	Ricoh_GX100	854	R1
4	Agfa_Sensor505 – x	172	A4	13	Nikon_D200	752	N2	22	Rollei_RCP – 7325XS	589	RO1
5	Agfa_Sensor530s	372	A5	14	Nikon_D70	369	N3	23	Samsung_L74wide	686	S1
6	Canon_Ixus55	224	C1	15	Nikon_D70s	367	N4	24	Samsung_NV15	645	S2
7	Canon_Ixus70	567	C2	16	Olympus_mju_1050SW	1040	O1	25	Sony_DSC – H50	541	SO1
8	Canon_PowerShotA640	188	C3	17	Panasonic_DMC – FZ50	931	P1	26	Sony_DSC – T77	725	SO2
9	Casio_EX – Z150	925	C4	18	Pentax_OptioA40	638	P2	27	Sony_DSC – W170	405	SO3

TABLE I: The Dresden image collection.

where c_{ij} is the count of images known to be from model C_i but predicted to be from model C_j. The counts can be converted to the conditional probability as,

$$p_{i|j} = \frac{c_{ij}}{\sum_{k=1}^{N} c_{kj}}, \tag{22}$$

where $p_{i|j}$ indicates the probability of actually from model C_i when predicted to be from model C_j. All those conditional probabilities can be represented as a matrix,

$$P = \begin{pmatrix} p_{1|1} & p_{1|2} & \cdots & p_{1|N} \\ p_{2|1} & p_{2|2} & \cdots & p_{2|N} \\ \vdots & \vdots & \ddots & \vdots \\ p_{N|1} & p_{N|2} & \cdots & p_{N|N} \end{pmatrix}. \tag{23}$$

We analysis the model coupling relationships in two-folds. The first is the *intra-model coupling*, which captures the coupling relationships of itself. The second is the *inter-model coupling*, which describes the inter-model coupling relationships.

Firstly, we calculate the intra-model coupling probability gain. The intra-model coupling relationship of C_i to itself can be described with the conditional probability as,

$$\lambda_i = p_{i|i}, \tag{24}$$

where $p_{\cdot|\cdot}$ is defined in Formula.20. Then, the intra-model coupling probability gain of e_i to itself can be obtained as,

$$CPG1(e_i) = \lambda_i e_i. \tag{25}$$

Secondly, we consider the inter-model coupling relationships. The inter-model coupling relationships of model C_j to C_i can be characterized using the conditional probability as,

$$\mu_{i|j} = p_{i|j}, \tag{26}$$

and the inter-model coupling probability gain of C_j to C_i can be calculated as,

$$CPG2(e_i|e_j) = \mu_{i|j} e_j. \tag{27}$$

Finally, the coupled probability representation of e_i can be obtained via combining the intra-model coupling and inter-model coupling as,

$$\begin{aligned} CPR(e_i) &= e_i + \eta(CPG1(e_i) + \sum_{j=1, j\neq i}^{N} CPG2(e_i|e_j)) \\ &= e_i + \eta(\lambda_i e_i + \sum_{j=1, j\neq i}^{N} \mu_{i|j} e_j) \\ &= e_i + \eta(p_{ii} e_i + \sum_{j=1, j\neq i}^{N} p_{i|j} e_j) \\ &= e_i + \eta(\sum_{j=1}^{N} p_{i|j} e_j), \end{aligned} \tag{28}$$

where η is the introduced adjustment factor to adjust the influence of overall model coupling probability gain. The left part of the Formula.28, $\sum_{j=1}^{N} p_{i|j} e_j$, shows that the conditional probabilities induced from the confusion matrix are integrated following the law of total probability.

Accordingly, the coupled probability representation of $\vec{e}$ can be expressed as,

$$\begin{aligned} CPR(\vec{e}) &= [CPR(e_1), \cdots, CPR(e_N)] \\ &= [e_1 + \eta(\sum_{j=1}^{N} p_{1|j} e_j, \cdots, e_N + \eta(\sum_{j=1}^{N} p_{N|j} e_j] \\ &= \vec{e} + \eta \vec{e} \otimes P^T, \end{aligned} \tag{29}$$

where $\otimes$ denotes the matrix multiplication.

V. Experiments and results

A large number of experiments were carried on a real-world image collection to evaluate the performance of the proposed scheme. This section reports the experiments and results.

A. Dataset, feature and setting

In this paper, the Dresden image collection [42] is used for the empirical study. The open image collection was specifically built for the purpose of development and benchmarking of camera-based digital forensic techniques. It was created using different scenes of natural and urban environments as well as indoor and outdoor environments. Table.I summarises the camera models, the number of images of each model and the aliases of camera models. To explore various situations, we construct three image sets: Set A, Set B, Set C, which are depicted in detail as follows.

- *Set A*: A1, A2, A3, A4, A5, C1, C2, C3, C4, F1, K1, N1, N2, N3, N4;

Feature	Dimension	Alias
Average Pixel Value (R, G, B)	3	AP1~AP3
RGB Pairs Correlation (RG, RB, GB)	3	PC1~PC3
Neighbor Distribution Center of Mass (R, G, B)	3	CM1~CM3
RGB Pairs Energy Ratio (GB, GR, BR)	3	PE1~PE3
RGB Pairs Energy Ratio (GB, GR, BR)	9	WS1~WS9
Pixel Difference based Image Quality Metrics	4	PD1~PD4
Correlation based Image Quality Metrics	3	C1~C3
Spectral Distance based Image Quality Metrics	6	SD1~SD6

TABLE II: The image features.

- *Set B*: O1, P1, P2, P3, PR1, R1, RO1, S1, S2, SO1, SO2, SO3;
- *Set C*: All models.

We extracted 34 features proposed by Kharrazi *et al.* [7] for the identification task. The features were generated by using the source code provided by Kharrazi *et al.* [7]. Table.II summarises the features, the dimensions and aliases. Finally, an image was represented by a feature vector of 34 dimensions.

For each image set, 30% percent of all images are randomly selected as training dataset. The remaining are treated as testing dataset. We used the LIBSVM [40] to solve SVMs. Linear kernels were applied in our experiments.

B. Evaluation metrics

We use accuracy and F-measure to measure the performance of image source identification.

- Accuracy is defined as the ratio of the number of all correctly identified images to the number of all identified images.

$$\text{Accuracy} = \frac{\#\text{ correctly identified images}}{\#\text{ identified images}}. \quad (30)$$

- F-measure [43] is used to measure the identification performance of a camera model C_i, which is a combination of precision and recall.

$$\text{F}-\text{measure}^{\text{i}} = 2 \cdot \frac{\text{precision}^{\text{i}} \cdot \text{recall}^{\text{i}}}{\text{precision}^{\text{i}} + \text{recall}^{\text{i}}}. \quad (31)$$

where $\text{precision}^{\text{i}}$ is the ratio of the number of correctly identified images from C_i to the number of images identified from C_i.

$$\text{precision}^{\text{i}} = \frac{\#\text{ correctly identified images from } \text{C}_{\text{i}}}{\#\text{ images identified from } \text{C}_{\text{i}}}. \quad (32)$$

and recall^{i} is defined as the ratio of the number of correctly identified images from C_i over the total of images from C_i.

$$\text{recall}^{\text{i}} = \frac{\#\text{ correctly identified images from } \text{C}_{\text{i}}}{\#\text{images from } \text{C}_{\text{i}}}. \quad (33)$$

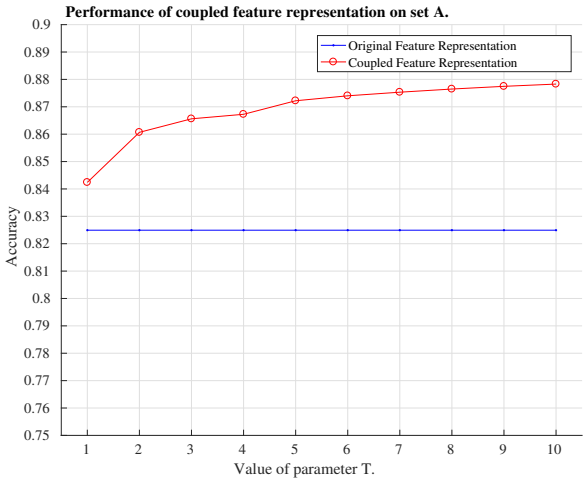

Fig. 4: Performance of coupled feature representation on set A.

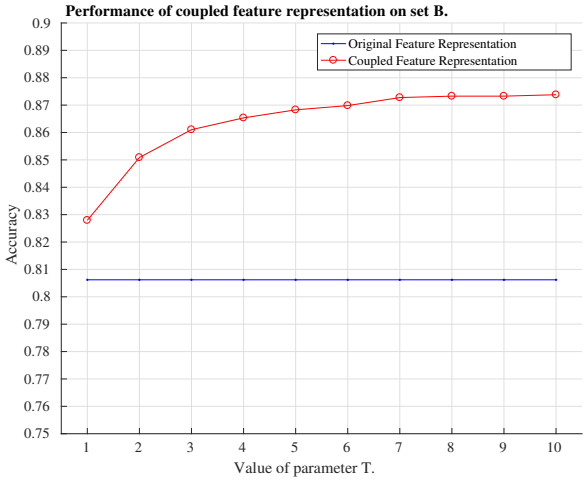

Fig. 5: Performance of coupled feature representation on set B.

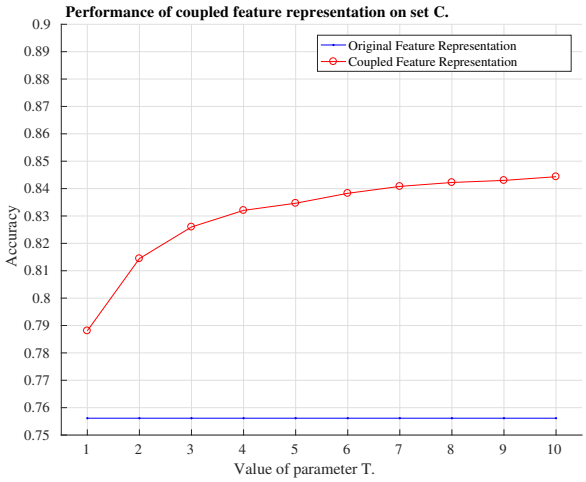

Fig. 6: Performance of coupled feature representation on set C.

C. Evaluation of Coupled Feature Representation

In this experiment, we evaluate the performance of the proposed coupled feature representation. The original feature representation adopted in previous [6–10] was implemented as reference. In the proposed coupled feature representation, there is a parameter, T, the largest power defined in Formula.6. To evaluate the influence of T, the coupled feature representation was implemented with T varying from 1 to 10.

Figure.4, Figure.5 and Figure.6 show the experimental results of the two representation methods on set A, B, and C respectively. We can see that the proposed coupled feature representation can significantly improve the identification accuracy. For example, on set A, with parameter $T = 6$, the identification accuracy of coupled feature representation is 87.4%, while the original feature representation is 82.4%. On set C, when $T = 4$, the identification accuracy of coupled feature representation can be improved to 83.2%, while the original feature representation is only 75.6%. The reason for the performance improvement of coupled feature representation is that it can successfully capture the intrinsic linear and non-linear feature coupling relationships, while the original feature representation overlooks this point.

From the figures, we also can see that the parameter T has great influence on the performance improvement. As a general trend, the identification accuracy goes up as when T increase. But the increase rate get smaller as T grows. This is consistent with Formula.9 and Formula.12, since the features with larger power have less coupling gain contribution. In the experiments followed, we fix T to be 4 to balance the computation cost and identification accuracy.

D. Evaluation of Coupled Probability Representation

This experiment was carried out to validate the effectiveness of the proposed coupled probability representation. The original feature representation, and coupled feature representation without coupled probability representation were implemented as references. Coupled probability representation was implemented with parameter η (defined in Formula.28) varying from 2^{-3} to 2^{6}.

The experimental results on set A, B and C are reported in Figure.7, Figure.8 and Figure.9 respectively. It is shown that the couped probability representation can further improve the identification performance. For example, on set C, with $\eta = 64$, the accuracies of original feature representation, coupled feature representation and coupled feature representation plus coupled probability representation are 82.5%, 86.6% and 87.8%, respectively. On set C, the accuracies of the three comparetives are 75.6%, 83.2% and 85.5% respectively. We can see that the performance improvement on set C is larger than that on set A. The reason is that set C contains more models than set A, and the model coupling information of set C is richer than set A.

Let's further investigate the influence of parameter η. In general, the identification accuracy goes up with bigger η. This is because more coupling information are integrated in the coupled probability representation. When η is big,

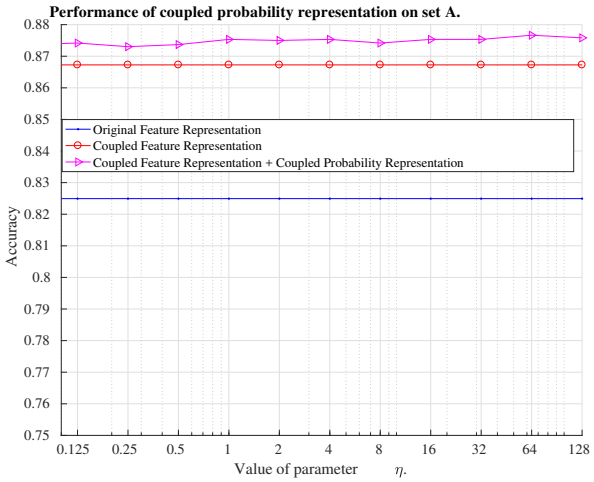

Fig. 7: Performance of coupled probability representation on set A.

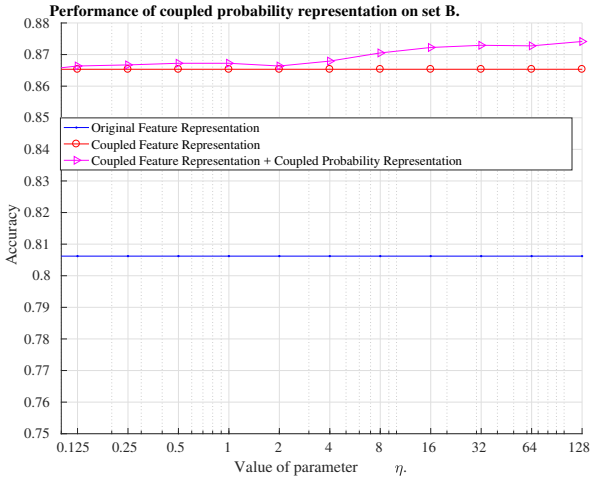

Fig. 8: Performance of coupled probability representation on set B.

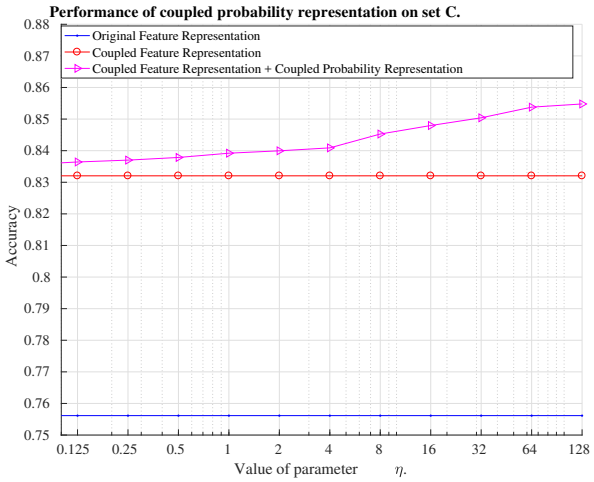

Fig. 9: Performance of coupled probability representation on set C.

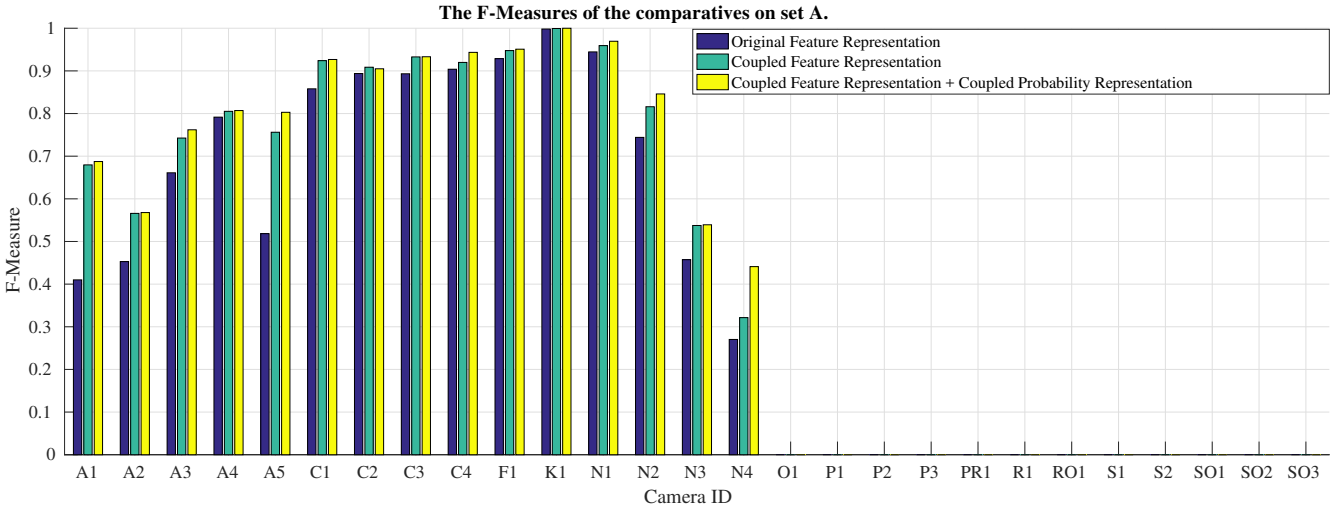

Fig. 10: The F-measure of the compared solutions on set A.

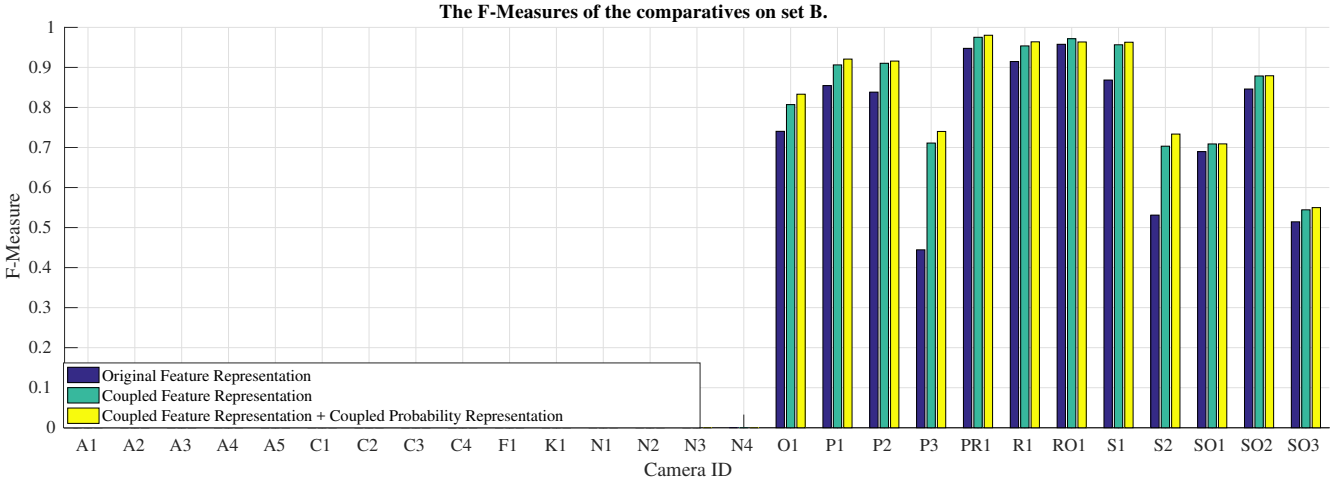

Fig. 11: The F-measure of the compared solutions on set B.

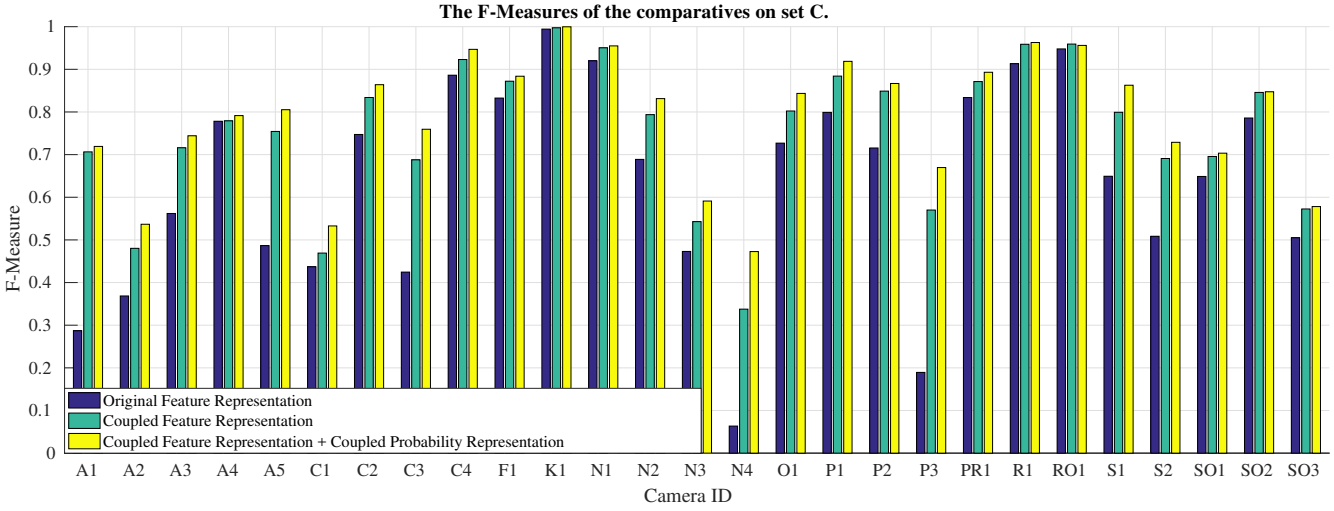

Fig. 12: The F-measure of the compared solutions on set C.

the identification accuracy becomes stable. In our further experiments, η is set to 64.

E. Evaluation with F-Measures

The goal of this experiment is to investigate the performance of the proposed solution in terms of F-Measures. The results are reported in Figure.10, Figure.11 and Figure.12 respectively. We can see that the results are consistent with that in Section.V-D.

For most models, the F-Measures of coupled feature representation plus coupled probability representation is superior to only coupled feature representation. And coupled feature representation is better than original feature representation. For example, on set A, the F-Measures of the three methods for N4 are 27%, 32% and 44% respectively. On set C, the F-Measures of C1 are 44%, 46% and 53% respectively.

From the figures, we also can see that the coupled models tend to have better performance improvement. For example, on set C, model N3 and N4 have bigger accuracy improvement than the average, and they are coupled as shown in Figure.2.

VI. Conclusion

This paper addressed the issues of feature coupling and model coupling for image source identification. To our best knowledge, we are the first to identify and solve both the two problems. The existing of feature coupling is because that image features characterize the hardware or software-related fingerprints from different views, and are naturally related to each other in some ways. For the models produced by the same manufacturer, the hardware infrastructure and image processing algorithms of them tend to be similar, causing the model coupling. In this paper, we demonstrated the two phenomenons with experimental results on a real-word dataset. A new image identification scheme is also developed to address the two issues. In the proposed solution, the feature coupling relationships are captured with coupled feature representation, and a new coupled probability representation is developed to deal with model coupling. To evaluate the new scheme, a large number of experiments were carried out on a real-world image collection. The results demonstrate that the both coupled feature representation and coupled probability representation can contribute to identification performance improvement.

Acknowledgment

This work is supported by the National Natural Science Foundation of China (No. 61300077).

References

[1] M. C. Stamm and K. J. R. Liu, "Forensic detection of image manipulation using statistical intrinsic fingerprints," *IEEE Transactions on Information Forensics and Security*, vol. 5, no. 3, pp. 492–506, 2010.

[2] Z. Deng, A. Gijsenij, and J. Zhang, "Source camera identification using auto-white balance approximation," in *The 13th IEEE International Conference on Computer Vision*, Barcelona, Spain, 2011, pp. 57–64.

[3] Camera and Imaging Products Association Standardization Committee and others,"Exchangeable image file format for digital still cameras: EXIF Version 2.3," Tech. Rep, 2010.

[4] I. J.Cox, M. L. Miller, and J. A. Bloom, *Digital Watermarking*. San Francisco, CA, USA: Morgan Kaufmann Publishers Inc., 2002.

[5] R. Schyndel, A. Z. Tirkel, and C. F. Osborne, "A digital watermark," in *The 1st IEEE International Conference Image Processing*, vol. 2, Austin, Texas, USA, 1994, pp. 86–90.

[6] S. Bayram, H. Sencar, N. Memon, and I. Avcibas, "Source camera identification based on CFA interpolation," in *The 12th IEEE International Conference on Image Processing*, vol. 3, Genoa, Italy, 2005, pp. 69–72.

[7] M. Kharrazi, H. T. Sencar, and N. Memon, "Blind source camera identification," in *The 11th IEEE International Conference on Image Processing*, Singapore, 2004, pp. 709–712.

[8] O. Çeliktutan, B. Sankur, and I. Avcibaş, "Blind identification of source cell-phone model," *IEEE Transactions on Information Forensics and Security*, vol. 3, no. 3, pp. 553–566, 2008.

[9] F. Peng, J. Shi, and M. Long, "Comparison and analysis of the performance of PRNU extraction methods in source camera identification," *Journal of Computational Information Systems*, vol. 9, no. 14, pp. 5585–5592, 2013.

[10] A. Castiglione, G. Cattaneo, M. Cembalo, and U. F. Petrillo, "Experimentations with source camera identification and online social networks," *Journal of Ambient Intelligence and Humanized Computing*, vol. 4, no. 2, pp. 265–274, 2013.

[11] C. Cortes and V. Vapnik, "Support-vector networks," *Machine Learning*, vol. 20, no. 3, pp. 273–297, 1995.

[12] J. Lukáš, J. Fridrich, and M. Goljan, "Digital camera identification from sensor pattern noise," *IEEE Transactions on Information Forensics and Security*, vol. 1, no. 2, pp. 205–214, 2006.

[13] Y. Sutcu, S. Bayram, H. T. Sencar, and N. Memon, "Improvements on sensor noise based source camera identification," in *The 2007 IEEE International Conference on Multimedia and Expo*, Beijing, China, 2007, pp. 24–27.

[14] C. T. Li, "Source camera identification using enhanced sensor pattern noise," *IEEE Transactions on Information Forensics and Security*, vol. 5, no. 2, pp. 280–287, 2010.

[15] C. T. Li and Y. Li, "Color-decoupled photo response non-uniformity for digital image forensics," *IEEE Transactions on Circuits and Systems for Video Technology*, vol. 22, no. 2, pp. 260–271, 2012.

[16] X. Kang, Y. Li, Z. Qu, and J. Huang, "Enhancing source camera identification performance with a camera reference phase sensor pattern noise," *IEEE Transactions on Information Forensics and Security*, vol. 7, no. 2, pp. 393–402, 2012.

[17] X. Kang, J. Chen, K. Lin, and A. Peng, "A context-adaptive SPN predictor for trustworthy source camera

identification," *EURASIP Journal on Image and Video Processing*, vol. 2014, no. 1, pp. 1–11, 2014.

[18] M. J. Tsai, C. S. Wang, J. Liu, and J. S. Yin, "Using decision fusion of feature selection in digital forensics for camera source model identification," *Computer Standards & Interfaces*, vol. 34, no. 3, pp. 292–304, 2012.

[19] K. S. Choi, E. Y. Lam, and K. K. Wong, "Automatic source camera identification using the intrinsic lens radial distortion," *Optics Express*, vol. 14, no. 24, pp. 11 551–11 565, 2006.

[20] K. S. Choi and E. Y. Lam, "Source camera identification using footprints from lens aberration," in *Proceedings of SPIE*, 2006, pp. 60 690J1–60 690J8.

[21] M. G. Hwang, H. J. Park, and D. H. Har, "Source camera identification based on interpolation via lens distortion correction," *Australian Journal of Forensic Sciences*, vol. 46, no. 1, pp. 98–110, 2014.

[22] L. T. Van, S. Emmanuel, and M. S. Kankanhalli, "Identifying source cell phone using chromatic aberration," in *The 2007 IEEE International Conference on Multimedia and Expo*, Beijing, China, 2007, pp. 883–886.

[23] A. E. Dirik, H. T. Sencar, and N. Memon, "Digital single lens reflex camera identification from traces of sensor dust," *IEEE Transactions on Information Forensics and Security*, vol. 3, no. 3, pp. 539–552, 2008.

[24] A. E. Dirik and H. T. Sencar, "Source camera identification based on sensor dust characteristics," in *The 2007 IEEE Workshop on Signal Processing Applications for Public Security and Forensics*, Washington, DC, USA, 2007, pp. 1–6.

[25] Z. J. Geradts, J. Bijhold, M. Kieft, K. Kurosawa, K. Kuroki, and N. Saitoh, "Methods for identification of images acquired with digital cameras," in *Enabling Technologies for Law Enforcement*, 2001, pp. 505–512.

[26] L. Bondi, L. Baroffio, D. Güera, P. Bestagini, E. J. Delp, and S. Tubaro, "First steps toward camera model identification with convolutional neural networks," *IEEE Signal Processing Letters*, vol. 24, no. 3, pp. 259–263, 2017.

[27] L. Bondi, D. Güera, L. Baroffio, P. Bestagini, E. J. Delp, and S. Tubaro, "A preliminary study on convolutional neural networks for camera model identification," *Electronic Imaging*, vol. 2017, no. 7, pp. 67–76, 2017.

[28] A. Tuama, F. Comby, and M. Chaumont, "Camera model identification with the use of deep convolutional neural networks," in *2016 IEEE International Workshop on Information Forensics and Security*, Abu Dhabi, United Arab Emirates, 2016, pp. 1–6.

[29] F. D. O. Costa, E. Silva, M. Eckmann, W. J. Scheirer, and A. Rocha, "Open set source camera attribution and device linking," *Pattern Recognition Letters*, vol. 39, pp. 92–101, 2014.

[30] Y. Huang, J. Zhang, and H. Huang, "Camera model identification with unknown models," *IEEE Transactions on Information Forensics and Security*, vol. 10, no. 12, pp. 2692–2704, 2015.

[31] G. J. Bloy, "Blind camera fingerprinting and image clustering," *IEEE Transactions on Pattern Analysis and Machine Intelligence*, vol. 30, no. 3, pp. 532–534, 2008.

[32] R. Caldelli, I. Amerini, F. Picchioni, and M. Innocenti, "Fast image clustering of unknown source images," in *2010 IEEE International Workshop on Information Forensics and Security*, Seattle, WA, USA, 2010, pp. 1–5.

[33] C. T. Li, "Unsupervised classification of digital images using enhanced sensor pattern noise," in *Proceedings of 2010 IEEE International Symposium on Circuits and Systems*, Paris, France, 2010, pp. 3429–3432.

[34] I. Amerini, R. Caldelli, P. Crescenzi, A. D. Mastio, and A. Marino, "Blind image clustering based on the normalized cuts criterion for camera identification," *Signal Processing: Image Communication*, vol. 29, no. 8, pp. 831–843, 2014.

[35] B. b. Liu, H. K. Lee, Y. Hu, and C. H. Choi, "On classification of source cameras: A graph based approach," in *2010 IEEE International Workshop on Information Forensics and Security*, Seattle, WA, USA, 2010, pp. 1–5.

[36] F. Marra, G. Poggi, C. Sansone, and L. Verdoliva, "Blind prnu-based image clustering for source identification," *IEEE Transactions on Information Forensics and Security*, vol. 12, no. 9, pp. 2197–2211, 2017.

[37] G. Gan, C. Ma, and J. Wu, *Data clustering: theory, algorithms, and applications*. SIAM, 2007.

[38] C. Wang, Z. She, and L. Cao, "Coupled attribute analysis on numerical data," in *International Joint Conference on Artificial Intelligence*, Beijing, China, 2013.

[39] C. Wang, X. Dong, F. Zhou, L. Cao, and C. H. Chi, "Coupled attribute similarity learning on categorical data," *IEEE Transactions on Neural Networks and Learning Systems*, vol. 26, no. 4, pp. 781–797, 2015.

[40] C. Chang and C. Lin, "LIBSVM: a library for support vector machines," National Taiwan University, http://www.csie.ntu.edu.tw/~cjlin/libsvm/, accessed Jul. 15, 2017.

[41] T. F. Wu, C. J. Lin, and R. C. Weng, "Probability estimates for multi-class classification by pairwise coupling," *Journal of Machine Learning Research*, vol. 5, no. Aug, pp. 975–1005, 2004.

[42] T. Gloe and R. Böhme, "The Dresden image database for benchmarking digital image forensics," *Journal of Digital Forensic Practice*, vol. 3, no. 2-4, pp. 150–159, 2010.

[43] G. Hripcsak and A. S. Rothschild, "Agreement, the F-measure, and reliability in information retrieval," *Journal of the American Medical Informatics Association*, vol. 12, no. 3, pp. 296–298, 2005.